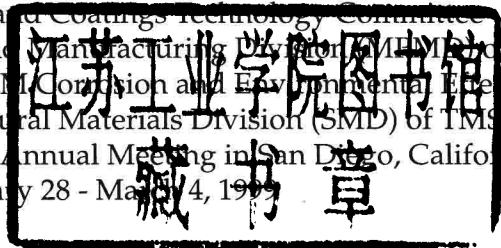


ELEVATED TEMPERATURE COATINGS:

Science and Technology III

Proceedings of a symposium sponsored by the
Surface Modification and Coatings Technology Committee
of the Materials Processing and Manufacturing Division (MPMD) of TMS,
and by the Joint TMS/ASM Corrosion and Environmental Effects
Committee of the Structural Materials Division (SMD) of TMS,
held during the 1999 TMS Annual Meeting in San Diego, California
February 28 - March 4, 1999



Edited by

Janet M. Hampikian

Narendra B. Dahotre

A Publication of
TMS

A Publication of
The Minerals, Metals & Materials Society
420 Commonwealth Drive
Warrendale, Pennsylvania 15086

Visit the TMS web site at
<http://www.tms.org>

The Minerals, Metals & Materials Society is not responsible for statements or opinions and is absolved of liability due to misuse of information contained in this publication.

Printed in the United States of America
Library of Congress Catalog Card Number 98-68628
ISBN Number 0-87339-421-6

Authorization to photocopy items for internal or personal use, or the internal or personal use of specific clients, is granted by The Minerals, Metals & Materials Society for users registered with the Copyright Clearance Center (CCC) Transactional Reporting Service, provided that the base fee of \$3.00 per copy is paid directly to Copyright Clearance Center, 27 Congress Street, Salem, Massachusetts 01970. For those organizations that have been granted a photocopy license by Copyright Clearance Center, a separate system of payment has been arranged.

TMS
Minerals • Metals • Materials

© 1999

If you are interested in purchasing a copy of this book, or if you would like to receive the latest TMS publications catalog, please telephone 1-800-759-4867 (U.S. only) or 724-776-9000, Ext. 270.

PREFACE

Elevated Temperature Coatings: Science and Technology III is the third volume in a series of invited and contributed papers presented in the symposium: "High Temperature Coatings III". This symposium was organized by Janet M. Hampikian and Narendra B. Dahotre, and held in San Diego, California, during the TMS annual meeting, February 28-March 4, 1999. This volume consists of invited and contributed papers from national and international researchers representing universities, federal laboratories and industries. Thus, it provides a rich diversity of material in the research area of High Temperature Coatings. The sponsorship of the TMS Surface Modification and Coatings Technology Committee, Materials Processing and Manufacturing Division, and the Joint TMS/ASM Corrosion and Environmental Effects Committee, Structural Materials Division, is gratefully acknowledged.

The motivation for holding a series of symposia on the topic of High Temperature Coatings is evident considering the current aim of achieving better surface characteristics (e.g. hardness, corrosiveness) from a wide range of materials without compromising bulk characteristics such as, for example, mechanical performance. An example of this is the current thrust toward achieving higher operating temperature in industrial gas turbine engine components through use of thermal barrier coatings in high temperature gradient areas such as experienced by turbine nozzles and blades. It should be noted that the platform provided by this symposium emphasizes the coating materials rather than the processes used to form them. Accordingly, specific materials topics covered include: Thermal Barrier Coatings, Overlay Coatings for Engine Applications, Coatings for Steels, Ceramic Coatings, and Intermetallic Coatings. This is an edited proceeding, and we thank the reviewers for their time, diligence and promptness in responding to our many requests. In particular, J.M.H. would like to thank A. Alexiou, T. Chen, J. Griffin and G. Grandinetti for their assistance.

We are grateful for the institutional support provided by the School of Materials Science and Engineering at the Georgia Institute of Technology, and the institutional support of the University of Tennessee Space Institute. We thank in particular Mrs. Teresa Bailey for her secretarial support. Finally, we appreciate the continuing assistance from TMS for this Symposium on High Temperature Coatings.

Dr. Janet M. Hampikian
School of Materials Science and Engineering
Georgia Institute of Technology
Atlanta, Georgia 30332-0245

Dr. Narendra B. Dahotre
Center for Laser Applications
Department of Materials Science and Engineering
The University of Tennessee Space Institute
Tullahoma, Tennessee 37388

TABLE OF CONTENTS

Preface	v
---------------	---

Thermal Barrier Coatings I

The Effect of Segregants on the Oxidation of the Bond Layer FeCrAl	3
<i>C. Mennicke, E. Schumann, E. Sommer, and M. Rühle</i>	
Evolution of Porosity and Texture in Thermal Barrier Coatings Grown by EB-PVD	13
<i>S.G. Terry, J.R. Litty, and C.G. Levi</i>	
Thermal Stability of an EB-PVD Thermal Barrier Coating System on a Single Crystal Nickel-Base Superalloy	27
<i>U. Kaden, C. Leyens, M. Peters, and W.A. Kaysser</i>	
Investigation of Damage Mechanisms in Thermal Barrier Coatings by Acoustic Emission	39
<i>F. Dettenwanger, H. Echsler, C. Burns, and M. Schütze</i>	

Thermal Barrier Coatings II

Mechanisms for the Failure of Electron Beam Physical Vapor Deposited Thermal Barrier Coatings Induced by High Temperature Oxidation	51
<i>M.J. Stiger, N.M. Yanar, F.S. Pettit, and G.H. Meier</i>	
Precursor to TBC Failure by Constrained Phase Transformation in the Thermally Grown Oxide	67
<i>D.R. Clarke, V. Sergo, and M.-Y. He</i>	
Hot Corrosion of Nickel-Base Alloys in Biomass Derived Fuel Simulated Atmosphere	79
<i>C. Leyens, I.G. Wright, and B.A. Pint</i>	
The Effect of Salt Chemistry on Superalloy Corrosion	91
<i>J.G. Smeggil</i>	
Oxidation Resistance of Ceramic Coatings Treated by Impulse Plasma Fluxes	103
<i>S.F. Korablev, I.R. Korableva, and A.R. Kopan</i>	

Mechanical Property Change of Zirconia Implanted by Y Ions	111
<i>J.-Z. Zhang, X.-Y. Ye, W.-J. Si, C. Guan, X. Zhang, and H. Zhang</i>	

Overlay Coatings for Engine Applications

The Significance of Bond Coat Oxidation for the Life of TBC Coatings	119
<i>W.J. Quadackers, A.K. Tyagi, D. Clemens, R. Anton, and L. Singheiser</i>	
Diffusion Barriers to Increase the Oxidative Life of Overlay Coatings	131
<i>J.A. Nesbitt and J.-F. Lei</i>	
Microstructures Resulting from MCrAlY Coating/Superalloy Interdiffusion	143
<i>F. Meisenkothen and J.E. Morral</i>	
Kinetic Considerations for Processing a Diffusion NiAl Coating Uniformly Doped with a Reactive Element by Chemical Vapor Deposition	149
<i>W.Y. Lee and G.Y. Kim</i>	
Mechanical Properties of YSZ-Alumina Thin Films Deposited via Combustion CVD	161
<i>D.W. Stollberg, W.B. Carter, J.M. Hampikian, K. Breder, and L. Riester</i>	
High Aspect Ratio Microstructure-Supported Shroud for a Turbine Blade	173
<i>K.W. Kelly</i>	
Effects of Platinum Additions and Sulfur Impurities on the Microstructure and Scale Adhesion Behavior of Single-Phase CVD Aluminide Bond Coatings	185
<i>J.A. Haynes, Y. Zhang, W.Y. Lee, B.A. Pint, I.G. Wright, and K.M. Cooley</i>	
Thermomechanical Fatigue of a Single Crystal Superalloy: Influence of a Protective Coating	197
<i>A. Sanz, L. Llanes, J.-P. Bernadou, and M. Anglada</i>	
Reactive Processing of a Dense Functionally-Graded Intermetallic Matrix Composite Coating	217
<i>H.X. Zhu and R. Abbaschian</i>	

Coatings for Steels

Microstructural Analysis and Performance Evaluation in Laser Cladding of Stainless Steel on the Surface of Plain Carbon Steel	231
<i>W. Guo and A. Kar</i>	
Evaluation of a Duplex Stainless Steel Coating Deposited on a Carbon Steel by the TIG Welding Process	243
<i>C.R. Xavier, A.L.B. Baptista, L.C.A. Vieira, E.L. Luiz, and P.R.F. Ribas</i>	

Elevated Temperature Oxidation Protection of Carbon Steel by Combustion Chemical Vapor Deposition	253
<i>M.R. Hendrick, S. Shanmugham, and A.T. Hunt</i>	
Use of the Spotface Technique to Reduce Assessing Time of the Painted Galvanized Steel Corrosion	265
<i>A.N.C. Costa, P.R.F. Ribas, I.C. da Silva, J.E.R. de Carvalho</i>	
Characterization and Tribological Behavior of Composite Boride Coating Deposited on Steel using Laser Surface Engineering	273
<i>A. Agarwal and N.B. Dahotre</i>	
Role of Rare Earth Oxide Coatings in High Temperature Oxidation of Austenitic Steels	285
<i>S. Seal, S.K. Roy, S.K. Bose, and S.C. Kuiry</i>	
A New Diffusion Coating Resistive to Hot Sulphuric Acid	297
<i>K. Jozwiak, A. Mlynarczak, J. Jakubowski, T. Gapinska, P. Grzesiak, and G. Mesmacque</i>	

Ceramic and Intermetallic Coatings

High Temperature Oxidation of $\text{Ni}_{50}(\text{Al},\text{Be})_{50}$	305
<i>R.J. Hanrahan, Jr., D.P. Butt, K.C. Chen, T.N. Taylor, C.J. Maggiore, and D.J. Thoma</i>	
Development of High Temperature Sulfidation Resistant Fe-Al Weld Overlay Coatings	317
<i>S.W. Banovic, J.N. DuPont, and A.R. Marder</i>	
The Deposition of Chromia, Chromia/Yttria, and Silica Coatings via Combustion CVD	329
<i>A.E. Alexiou, S. Shanmugham, and J.M. Hampikian</i>	
Hardening and Microstructure of Aluminum Metal Surface Prepared by Complex Alloying Technique	341
<i>M. Okutomi, A. Obara, and K. Tsukamoto</i>	
Reaction Formed Coatings for SiC Fibers in Ceramic Matrix Composites	351
<i>M. McNallan, Y. Gogotsi, and D. Ersoy</i>	
Development of a Diffusion Barrier Layer for High-Temperature Molybdenum Electrodes	361
<i>D.A. Buell, C. Suryanarayana, D.L. Williamson, J.J. Moore, and J. Disam</i>	
Prevention of Hydrogen Permeation in TiAl by Ion Implantation	371
<i>Y. Matsumoto, Y.-C. Zhu, J. Imamura, and N. Iwamoto</i>	

Silicon Carbide Coating on UO ₂ Pellet by a Combustion Reaction	381
<i>B.G. Kim, Y. Choi, J.W. Lee, Y.W. Lee, and D.S. Sohn</i>	
Superhardness Effects in the Si ₃ N ₄ /TiN Ceramic Nano-Multilayer Films	391
<i>J. Xu, M. Gu, G. Li, and P. Li</i>	

Addendum

Formation of High Chromium Surface Alloys on 2.25Cr-1Mo and 9Cr-1Mo Steels using a Single Step Laser Treatment to Improve their High Temperature Oxidation/Corrosion Resistance	399
<i>A.S. Khanna, R. Streiff, and K. Wissenbach</i>	
Subject Index	419
Author Index	423

Thermal Barrier Coatings I

THE EFFECT OF SEGREGANTS ON THE OXIDATION OF THE BOND LAYER FeCrAl

Carsten Mennicke, Eckart Schumann, Eric Sommer and Manfred Rühle

Max-Planck-Institut für Metallforschung
Seestr. 92, D-70174 Stuttgart, Germany

Abstract

The performance of thermal barrier coatings is determined predominantly by the behavior of the 1 μm thick oxide scale, formed beneath the zirconia layer. Several factors may affect the cracking behavior of that interface. These factors include the composition of the alloy substrate and the coatings as well as thermal stresses. Studies by advanced transmission electron microscopy (TEM) techniques reveal the microstructure, composition and bonding at the interfaces and regions close to interfaces in that area. The results will be reported and discussed using different models which are required for an explanation of the failure behavior. Segregation to the interface between the bond coat and the oxide scale and formation of stresses in the scale are expected to play a major role.

Introduction

Recent workshops on thermal barrier coatings (TBCs) suggest that TBCs comprise a system involving the substrate alloy, the bond coat, the TBC itself, and the thermally grown oxide (TGO) between the TBC and bond coat, as well as the environment. A systematic approach is needed to both control and enhance the performance. The spall life is generally dictated by a TGO growth. The failure mechanisms involve the TGO and the TGO/bond coat interface. All motivated by the residual compression in the thermally grown oxide. For that reason, the interfaces between the thermally grown oxide and the bond layer FeCrAl are studied in detail.

The lifetime of high-temperature materials in corrosive environments depends strongly on their resistance against high-temperature oxidation. Therefore, the technical application of these materials requires the formation of a protective, slow growing oxide scale. Fe20Cr5Al based alloys form thermodynamically stable α -Al₂O₃ scales with slow growth rates at temperatures above 1000 °C. A serious problem, particularly under cyclic temperature conditions, is the spallation of the oxide scale. The repeated exposure of the metal to the gas atmosphere leads to Al depletion in the alloy and, finally, to breakaway oxidation and failure of the material.

It is well known that doping the alloys with small additions (< 0.1 wt.%) of so-called reactive elements (RE) such as Y or Zr improve the spallation resistance dramatically (reactive element effect). It is known that in the absence of RE, a few ppm of S, which exists as a natural impurity in these materials, has a detrimental effect on the scale adhesion [1]. Regarding this effect, the RE are assumed to tie up the S by forming thermodynamically stable sulfides, thus preventing S from segregating to the metal/oxide interface of interfacial voids. Indeed, it could be shown that oxide scales grown on hydrogen annealed, RE-free FeCrAl-alloys with extremely low S content (less than 1 ppm) do not spall and have the same good oxidation resistance as Y-doped alloys up to oxidation times of 1800 h [2]. However, the question arises, as to whether the sulfur effect is the only possible mechanism by which Y improves the spallation resistance or whether other beneficial Y effects have to be taken into account. Therefore, we compared Y-doped and undoped FeCrAl with regard to scale morphology, microstructure and stresses in the oxide. To exclude effects of other dopants or impurities, model alloys with high purity have been investigated. In this study the characterization of alumina scales with TEM has been combined with stress measurements using optical fluorescence spectroscopy.

Experimental

The composition of the investigated FeCrAl model alloys is shown in Table I. The high purity of the alloys was ensured by the control of more than 70 elements, all of which have concentrations of less than 3 ppm [3]. Metal pieces of 1 mm thickness were polished down to a ¼ µm diamond finish and ultrasonically cleaned in acetone before oxidation. The specimens were oxidized at 1200 °C for 5 h in air.

Scanning electron microscopy (SEM) was applied in order to investigate the scale morphology. Cross-sectional specimens were prepared for TEM. the detailed procedure of sample preparation has been described elsewhere [4]. Conventional TEM studies were performed in a JEOL 2000 FX (200 kV). For the analytical studies a VG HB 501 STEM (100 kV) equipped with a field-emission gun and an EDS Ge detector was used.

Table I Composition of high purity model alloys

Alloy	Fe	Cr (wt.%)	Al (wt.%)	Y (wt.%)	S (ppm)
A	bal	20.2	5.0	-	2
B	bal	19.9	5.0	-	45
C	bal	19.7	5.0	0.093	3
D	bal	20.0	4.9	0.080	15

The stress measurements were performed on alloys A (low S, no Y) and C (low S, with Y). They were oxidized at temperatures between 1100 °C and 1400 °C. The oxidation time was chosen so that, for all temperatures, a scale thickness of approximately 2 µm was achieved (Table II). After oxidation, the specimens were removed from the hot furnace and cooled to room temperature in a few minutes. For the temperature range above 800 °C cooling rates of about 30 K/s were estimated. For a given temperature, alloy A and C were always oxidized in the same exposure, so that both specimens have exactly the same cooling rate.

Stress measurements in the oxide scale were carried out using optical fluorescence of Cr-doped α -Al₂O₃. In the α -Al₂O₃ lattice trace impurities of Cr³⁺ substitute for Al³⁺. The electron relaxation processes, following excitation with a laser, give rise to two radiative electron transitions in the red optical spectrum, the so-called R1 and R2 ruby fluorescence lines. Deformation of the alumina lattice due to stress causes an energy shift relative to the unstressed crystal. The dependence of the frequency shift $\Delta\nu$ from the stress tensor σ can be approximated by a linear relationship [5,6]. For a randomly oriented, polycrystalline material with small grain size compared to the excited volume, Ma and Clarke [5] have calculated the average value of $\Delta\nu$:

$$\overline{\Delta\nu} = \frac{1}{3}(\Pi_{xx} + \Pi_{yy} + \Pi_{zz})(\sigma_{xx} + \sigma_{yy} + \sigma_{zz}) \quad (1)$$

where Π_{ii} are the diagonal elements of the piezospectroscopic tensor. The tensor trace $\Pi_{xx} + \Pi_{yy} + \Pi_{zz}$ was experimentally determined by He and Clarke [6] to be 7.61 cm⁻¹/GPa for the R2 line. Assuming a two-dimensional stress state in the oxide plane with the z-axis normal to the metal/oxide interface with $\sigma_{xx} = \sigma_{yy} = \sigma, \sigma_{zz} = 0$ leads to

$$\sigma = \frac{3}{2} \cdot \frac{\overline{\Delta\nu}}{\Pi_{xx} + \Pi_{yy} + \Pi_{zz}} \quad (2)$$

Through this equation the stress in the oxide scale can be calculated when $\Delta\nu$ has been determined. Fluorescence spectra of the alumina scales were obtained by exciting the specimen with the 543 nm line of a 1.5 mW He-Ne laser which was focussed to a 10 µm spot on the oxide surface. The fluorescence signal was collected by a 0.85 meter double monochromator and a GaAs-photomultiplier. The peak frequency was determined by fitting a double Lorentzian function to the experimental spectra.

Table II Oxidation times and temperatures of alloys A and Ca which were used for stress measurements

Temperature	1100 °C	1200 °C	1300 °C	1400 °C
Oxidation time	11.1 h	2.5 h	35 min	14 min

Results

Characterization of the Microstructure

Figure 1 shows SEM cross-sections for the alloys oxidized at 1200 °C for 5 h. The alumina scale thickness was for all specimens about 2.7 μm . The oxidation behavior of the samples without Y depended strongly on the S content. The low S alloy A (2 ppm S) showed a flat, adherent oxide scale whereas the high sulfur alloy B (45 ppm S) revealed a heavily convoluted scale. More than 30 % of the oxide on the high S specimen spalled during cooling. The uncovered metal surface showed many large voids with a smooth surface where the oxide has lost contact with the metal at temperature, whereas areas with oxide grain imprints indicate contact of the oxide to the substrate at temperature. Both Y-containing alloys C and D showed a flat, well adherent oxide scale. No spallation of the scale and no voids at the metal/oxide interface could be observed.

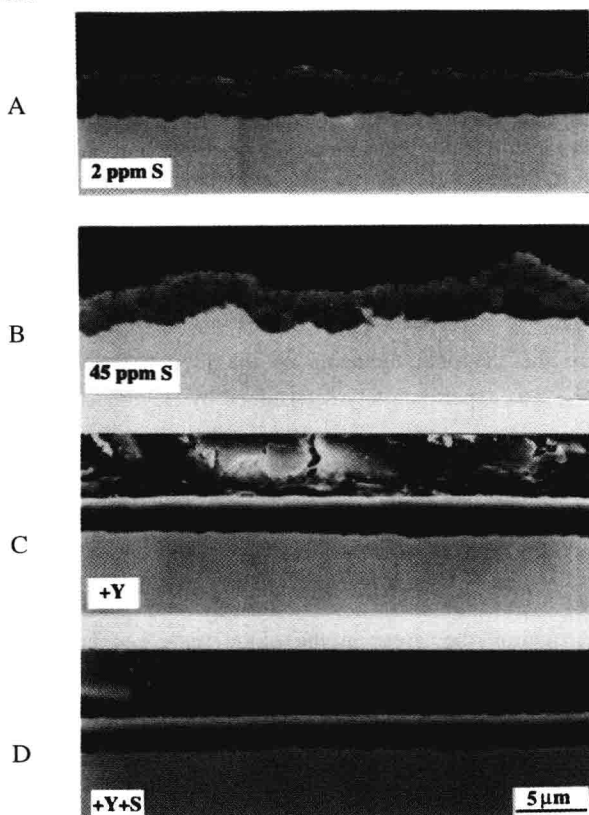


Figure 1 - SEM cross-sections of alloys A, B, C and D after oxidation for 5 h at 1200 °C

The grain structure of the oxide was studied with TEM. Figure 2 shows TEM cross-sections of the oxidized low sulfur specimens with and without Y (alloy C and A). The sample A showed large equiaxed $\alpha\text{-Al}_2\text{O}_3$ grains with a diameter of approximately $\frac{1}{2}$ - 1 μm . At the metal/oxide interface small voids were present at relative distances of a few microns, where an oxide grain boundary leads to the metal surface. Generally, the oxide grains were well in contact with the metal substrate. The Y-containing material had a columnar grain structure beneath a thin scale

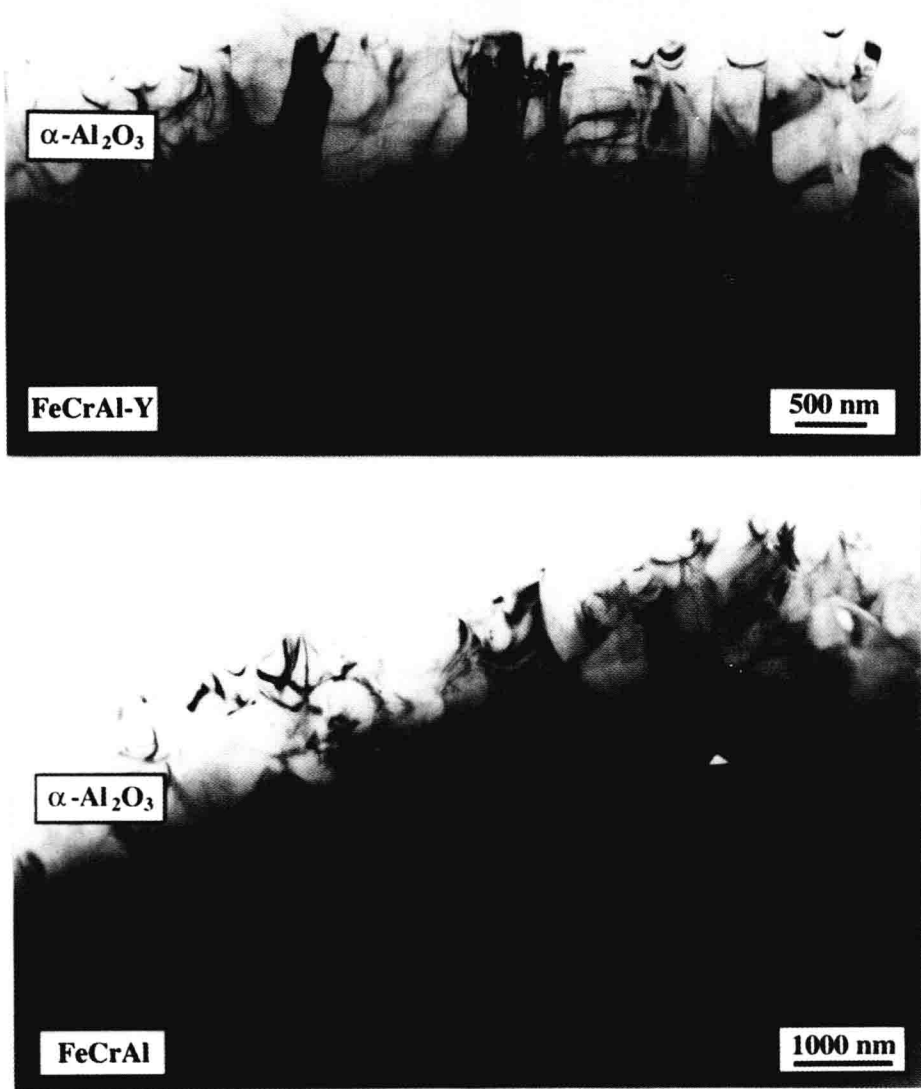


Figure 2 - TEM cross-sections of alloy C and A after oxidation at 1200 °C for 5 h

of small equiaxed grains at the gas/oxide interface. The formation of $\alpha\text{-Al}_2\text{O}_3$ was demonstrated by electron diffraction. The dimensions of the columnar grains were at least 1-2 μm in length and about 0.3-0.4 μm in width. Figure 3 shows a TEM micrograph of the columnar part of the oxide scale. At the oxide/metal interface no microvoids or precipitates were detectable. The small particles near the interface in the metal revealed a large Y content and are probably internal oxides.

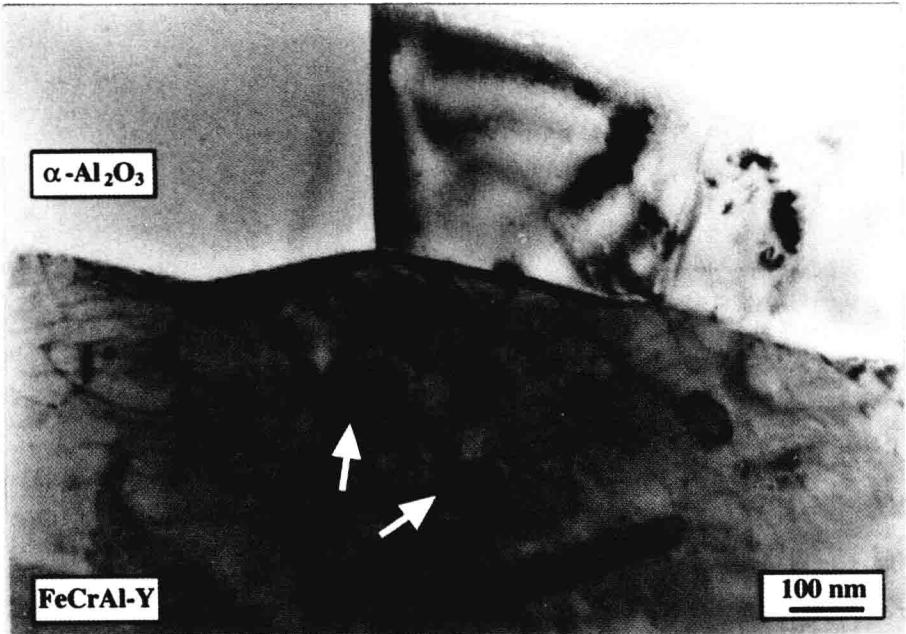


Figure 3 - TEM cross-section of alloy C after oxidation at 1200 °C for 5 h

More than 20 grain boundaries of each sample were investigated with STEM-EDS. A clear Y signal was detected at all examined grain boundaries for both specimens C and D. Figure 4a

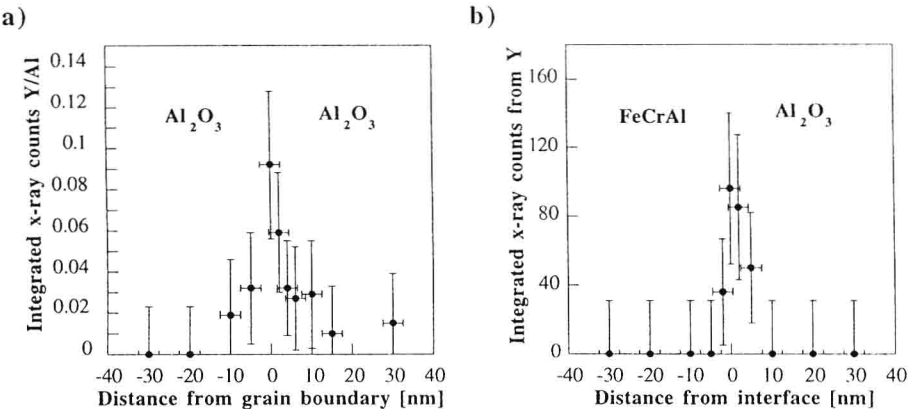


Figure 4 - STEM/EDS spot measurements at a) oxide grain boundary on alloy C and b) at the metal/oxide interface of alloy D after oxidation for 5 h at 1200°C

shows a set of spot measurements performed in a line perpendicular to the "edge-on" oriented grain boundary at varying distances. Y segregation was found at all grain boundaries. EDS measurements at the metal/oxide interface showed also Y segregation (Fig. 4b). No S signal above the detection limit of 0.1 monolayers could be detected.

Stress Measurements

Figure 5 shows typical measured fluorescence signals which were used for stress determination of the alumina scale. The R2 frequency of the spectrum of an unstressed piece of oxide which spalled off during cooling was used as reference (14432.7 cm^{-1}). The shifted spectrum of an adherent piece of oxide indicates compressive stresses of 4.9 GPa. The absolute stresses in the oxide on alloys A (no Y) and C (with Y) are given in Fig. 6 versus the oxidation temperature. The dotted line represents the calculated stress due to cooling as discussed in the next chapter. The Y containing scales withstood stresses more than 6 GPa without spallation. The scales without Y spalled in only a few small areas.

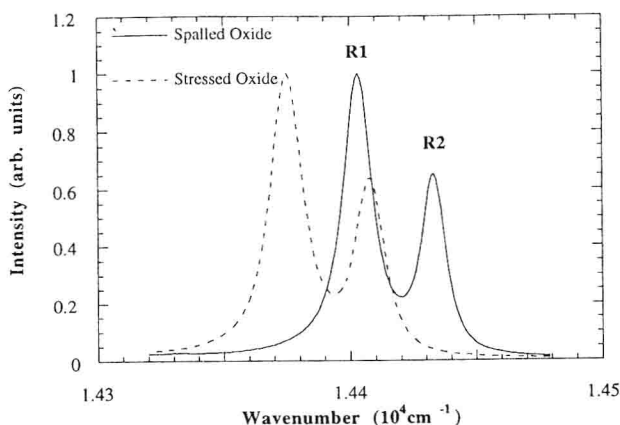


Figure 5 - R1/R2 fluorescence lines of polycrystalline $\alpha\text{-Al}_2\text{O}_3$ scales from a spalled piece of oxide on alloy B and from a stressed adherent oxide on alloy A with 4.9 GPa compressive stress

It was shown that this leads to a local stress release. Fluorescence measurements were therefore always made at least 200 μm from a spalled region. The standard deviation of stress measurements at different places on the same sample was always less than 3 % indicating a homogeneously lateral stress distribution. For the oxidation temperatures of 1100 $^\circ\text{C}$ and 1200 $^\circ\text{C}$ compressive stresses of the same magnitude occurred for both specimens, whereas for higher temperatures the Y-doped scales exhibited significantly higher stresses than in the undoped oxide.

Discussion

The spallation of the oxide on undoped FeCrAl, containing S levels higher than a few ppm, is generally explained by the segregation of S to the metal/oxide interface or to interfacial voids. There is still some discussion as to whether S segregates to the intact metal/oxide interface [7] weakening the bond between oxide and metal, or whether S can only segregate to the metal/gas